Original Article

JCBFM

Journal of Cerebral Blood Flow & Metabolism
2020, Vol. 40(2) 404–419

DOI: 10.1177/0271678X18818298
journals.sagepub.com/home/jcbfm
SAGE

Balanced single-vector co-delivery of VEGF/PDGF-BB improves functional collateralization in chronic cerebral ischemia

Aiki Marushima[1], Melina Nieminen[1], Irina Kremenetskaia[1], Roberto Gianni-Barrera[2], Johannes Woitzik[1], Georges von Degenfeld[3], Andrea Banfi[2], Peter Vajkoczy[1,*] and Nils Hecht[1,*]

Abstract

The myoblast-mediated delivery of angiogenic genes represents a cell-based approach for targeted induction of therapeutic collateralization. Here, we tested the superiority of myoblast-mediated co-delivery of vascular endothelial growth factor-A (VEGF) together with platelet-derived growth factor-BB (PDGF-BB) on transpial collateralization of an indirect encephalomyosynangiosis (EMS) in a model of chronic cerebral ischemia. Mouse myoblasts expressing a reporter gene alone (empty vector), VEGF, PDGF-BB or VEGF and PDGF-BB through a single bi-cistronic vector (VIP) were implanted into the temporalis muscle of an EMS following permanent ipsilateral internal carotid artery occlusion in adult, male C57BL/6N mice. Over 84 days, myoblast engraftment and gene product expression, hemodynamic impairment, transpial collateralization, angiogenesis, pericyte recruitment and post-ischemic neuroprotection were assessed. By day 42, animals that received PDGF-BB in combination with VEGF (VIP) showed superior hemodynamic recovery, EMS collateralization and ischemic protection with improved pericyte recruitment around the parenchymal vessels and EMS collaterals. Also, supplementation of PDGF-BB resulted in a striking astrocytic activation with intrinsic VEGF mobilization in the cortex below the EMS. Our findings suggest that EMS surgery together with myoblast-mediated co-delivery of VEGF/PDGF-BB may have the potential to serve as a novel treatment strategy for augmentation of collateral flow in the chronically hypoperfused brain.

Keywords

Collateral circulation, gene therapy, moyamoya disease, neurosurgery, revascularization

Received 24 August 2018; Revised 11 November 2018; Accepted 14 November 2018

Introduction

Patients with chronic cerebral hemodynamic impairment due to progressive stenosis or occlusion of major cerebral arteries carry a risk of recurrent transient ischemic attacks and cerebral infarction up to 20–30% at two years.[1,2] Direct extra- to intracranial bypass grafting with augmentation of collateral flow was expected to reduce this risk of subsequent ischemic stroke but surprisingly failed to show a benefit compared to best medical management, most likely due to the high procedure-related perioperative stroke rate up to 15% within the first 30 days following surgery.[1,3]

[1]Department of Neurosurgery and Center for Stroke research Berlin (CSB), Charité – Universitätsmedizin Berlin, Berlin, Germany
[2]Department of Biomedicine, University Hospital Basel and University of Basel, Basel, Switzerland
[3]Global Medical Affairs, Bayer Pharma AG, Wuppertal, Germany
*These authors contributed equally to this work.

Corresponding author:
Peter Vajkoczy, Department of Neurosurgery & Center for Stroke Research Berlin (CSB), Charité – Universitätsmedizin Berlin, Charitéplatz 1, 10117 Berlin, Germany.
Email: peter.vajkoczy@charite.de

An encephalomyosynangiosis (EMS) represents a simple and safe alternative to direct bypass surgery for treatment of chronic cerebral hemodynamic impairment and describes a technique, where a vascularized pedicle graft of the temporalis muscle is placed in direct contact with the surface of the hypoperfused brain after removal of the bone and dura.[4,5] However, hemodynamic rescue following the spontaneous formation of transpial extra- to intracranial collaterals between the muscle/brain interface of an EMS is not immediate and appears to be effective only in pediatric patients with moyamoya vasculopathy and high endogenous pro-angiogeinic activity[6–10] and not in adults with hemodynamic compromise due to arteriosclerotic cerebrovascular disease.[11,12] Importantly, effective collateralization through an EMS not only requires remodeling and outgrowth of *pre-formed* collateral vessels – arteriogenesis in the classical sense – but also de novo growth and maturation of an entirely new vascular network following mechanisms of postnatal vasculo- and angiogenesis, which precede the formation of patent and functional collaterals between the extracranial and intracranial vascular beds.

Here, vascular endothelial growth factor-A (VEGF) delivered at an appropriate microenvironmental concentration was shown to act as a key regulator of formation and maintenance of the native collateral density in the brain, next to the role of VEGF as a factor to induce capillary arterialization and proliferation of preformed arteriolar-arterial vessel networks.[13–18] However, VEGF delivery alone may act as a negative regulator of vessel maturation,[19] which is determined by pericyte recruitment mainly controlled by platelet-derived growth factor-BB (PDGF-BB).[20,21] Against this background, we previously showed that a balanced, myoblast-mediated co-expression of VEGF and PDGF-BB using a single bi-cistronic vector, VIP, appears to provide superior conditions to harness the potency of VEGF for safe and effective induction of therapeutic neovascularization.[22–25] Together with an EMS, retrovirally transfected myoblasts appear to be the ideal drug delivery vehicle for targeted and specific stimulation of collateral vessel growth in chronic cerebral ischemia, based on their capacity to fuse with pre-existing host muscle fibers of the EMS and ensure a highly localized gene product delivery without the need for immune suppression or the propensity to proliferate in an uncontrolled manner.[17,18,23,25–29]

To overcome the limitations of VEGF single-factor delivery, we therefore tested the efficacy of a balanced, myoblast-mediated co-expression of both murine VEGF ($VEGF_{164}$) and human PDGF-BB (hPDGF-BB) on collateralization and ischemic protection in a mouse model of EMS revascularization and chronic cerebral ischemia.

Material and methods

Ethics statement

Experiments were permitted by the local ethics committee on animal research (Landesamt für Gesundheit und Soziales, Berlin, Germany. LAGeSO No. G 0186/16) and in conformity with the German Law for Animal Protection and the National Institute of Health Guidelines for Care and Use of Laboratory Animals. Experiments have been reported following the ARRIVE guidelines.

Cell culture and growth factor secretion

The isolation, cultivation and retroviral infection of primary C57BL/6 mouse myoblasts was performed as previously described.[23,25,27,30] Briefly, primary myoblasts were transduced with a constitutive LacZ-encoding retrovirus to express the β-galactosidase marker gene (empty vector (EV)). In addition, LacZ-encoded myoblasts were further transduced with retroviral vectors expressing murine $VEGF_{164}$ (designated VEGF), hPDGF-BB (designated PDGF), or both at a fixed ratio to each other from a bi-cistronic cassette through the encephalomyocarditis virus internal ribosomal entry site (IRES) (designated VIP for VEGF-IRES-PDGF) as previously described.[23] A truncated version of CD8a was co-expressed with $VEGF_{164}$ or hPDGF-BB from a similar bi-cistronic construct (VEGF- and PDGF-myoblasts) or from a separate promoter (VIP) as a cell surface marker of transduced cells. Early-passage myoblast clones were randomly isolated using a FacStar cell sorter (Becton Dickinson, San Jose, CA, USA), and single-cell isolation was confirmed visually. All myoblast populations were cultured in 5% CO_2 on collagen-coated dishes.

For optimal selection of myoblast populations based on previous functional and morphological results,[23] $VEGF_{164}$ and hPDGF-BB secretion were quantified in cell culture supernatants using specific ELISA kits (R&D Systems, Abingdon, UK) as described previously.[17,23] Myoblast populations were selected for implantation as follows: monoclonal VEGF myoblasts homogeneously secreting $61.0 \pm 2.9\,ng/10^6$ cells/day of $VEGF_{164}$, polyclonal PDGF-myoblasts secreting on average $45.7 \pm 2.4\,ng/10^6$ cells/day of hPDGF-BB and polyclonal VIP-myoblasts secreting an average amount of $58.9 \pm 5.8\,ng/10^6$ cells/day of $VEGF_{164}$ and $9.7 \pm 0.7\,ng/10^6$ cells/day of hPDGF-BB at a fixed ratio in each cell.

Animals and design

A total number of 292 male C57BL/6N mice (Charles River WIGA GmbH, Sulzfeld, Germany),

aged 10–12 weeks were randomized to the following experimental groups:

- *EV*: internal carotid artery occlusion (ICA-O) and EMS with implantation of EV myoblasts
- *VEGF*: ICA-O and EMS with implantation of $VEGF_{164}$-expressing myoblasts
- *PDGF*: ICA-O and EMS with implantation of hPDGF-BB-expressing myoblasts
- *VIP*: ICA-O and EMS with implantation of $VEGF_{164}$- and hPDGF-BB co-expressing myoblasts

Animals were randomized with the help of an online randomizing tool (https://www.randomizer.org). Along the course of the observation period up to 84 days, 44 animals were excluded due to procedure-related mortality (EV n = 12, VEGF n = 13, PDGF n = 11, VIP n = 8). For all procedures, mice were anesthetized with 70 mg/kg ketamine and 16 mg/kg xylazine, and body temperature was maintained at 37 °C. Ketamine and xylazine were selected based on our previous model validation[31] in order to minimize cardiovascular and respiratory effects on cerebral blood flow (CBF) that may occur with volatile anesthetics, opioids or benzodiazepines and hamper reliable assessment of the acetazolamide-specific cerebrovascular reserve capacity (CVRC). Mice were kept in an enriched environment with free access to food and water. Blinding for treatment and data analysis was ensured by coding the myoblasts before implantation. To determine group allocation, un-coding was performed after individual data analysis.

ICA-occlusion, EMS and myoblast implantation

The ICA-O was performed immediately before the EMS procedure at a time point defined as day 0. For ICA-O, the animal was positioned supine, and the right-sided ICA was permanently ligated with an 8/0 silk suture. Next, the animal was turned to prone position, and a right-sided craniectomy was performed along the superior temporal line to the temporal scull base, extending from the bregma to the lambdoid suture using a diamond-tip micro drill (Proxxon GmbH, Wartberg/Aist, Austria). The dura was completely excised along the margin of the craniectomy. To secure the temporal muscle above the cortical surface after myoblast implantation (see below), the overlying muscle fascia was sutured to the contralateral aponeurosis, and the skin was readapted with 6/0 Nylon as previously described.[28,29,31] For implantation, cultured EV-, VEGF-, PDGF- and VIP-myoblasts were trypsinized and re-suspended in phosphate-buffered saline with 0.5% bovine serum albumin. Five cell suspensions of 5 µl, each containing 5×10^5 myoblasts (equaling a total number of 25×10^5 cells) were implanted into the temporalis muscle using a Hamilton® microsyringe with a 26-gauge needle (Hamilton Co., Reno, NV, USA) during the EMS procedure on day 0.

Measurement of cerebral hemodynamics using laser speckle imaging

Resting CBF and acetazolamide-specific CVRC of the *affected* (right) hemisphere was determined on days 0, 7, 21, 42 and 84 with non-invasive laser speckle imaging (LSI). After positioning of the laser speckle device (MoorFLPI, Moor Instruments, Devon, England), a 5-min baseline measurement of cortical resting perfusion (CBF-Flux measured in arbitrary perfusion units) was recorded within a 6×4 mm region of interest over the right middle cerebral artery (MCA) territory, which permitted a combined arterial, venous and parenchymal perfusion and blood flow assessment. A 120-s CBF-Flux plateau was calculated as baseline perfusion. Next, 50 mg/kg acetazolamide (Diamox, Goldshield Pharmaceuticals Ltd., Surrey, England) was injected intraperitoneally, and the acetazolamide-specific CVRC was calculated as the percent perfusion change between the baseline plateau and a 120-s CBF-Flux plateau after a maximum rise in CBF flux.[29,31] (days 0–21: EV n = 21, VEGF n = 20, PDGF n = 22, VIP n = 23; day 42: EV n = 17, VEGF n = 15, PDGF n = 17, VIP n = 16; day 84: EV n = 8, VEGF n = 8, PDGF n = 8, VIP n = 9). The normalized resting perfusion at each time point (defined as 100%) and mean CVRC on day 0 were additionally determined in the *unaffected* (left) hemisphere.

MCA occlusion and cortical stroke volume assessment

The percentage of ipsilateral cortical infarction after 60-min MCA-O and 6-h reperfusion was assessed through magnetic resonance imaging (MRI) on days 21, 42 and 84. For temporary MCA-occlusion (MCA-O), animals were turned to supine position, and the midline neck incision was reopened. The carotid sheath was carefully dissected and the right ICA was incised distal to the site of the previous ICA-O. Next, a 7/0 silicone-rubber-coated monofilament (Doccol monofilament, length 20 mm, diameter with coating 0.21 ± 0.01 mm; Doccol cooperation, Sharon, MA, USA) was smoothly inserted up to the level of the ICA/MCA bifurcation. After 60 min, the filament was removed and the ICA was permanently ligated proximal to the incision. Six hours later, the volume of the ischemic cortical tissue and of the total cortex ipsilateral to the EMS was determined in a 7-tesla animal MRI (Bruker Pharmascan 70/16 with a 20 mm radio

frequency volume resonator, Bruker Biospin, Ettlingen, Germany) and analyzed with purpose-designed biomedical imaging software (Analyze 10.0, Biomedical Imaging Resource, Mayo Clinic, Rochester, MN, USA) to determine the percentage of cortical infarction according to signal hyperintensity in serial T2-weighted coronal images.[29] LSI was used to visualize the cortical perfusion pattern over the affected hemisphere during the 60-min occlusion. Correlation between the percentage of cortical infarction and CVRC was analyzed to assess the effect of the hemodynamic response following EMS and VIP-myoblast implantation (day 21: EV n = 5, VEGF n = 6, PDGF n = 6, VIP n = 6; day 42: EV n = 7, VEGF n = 6, PDGF n = 7, VIP n = 7; day 84: EV n = 6, VEGF n = 8, PDGF n = 5, VIP n = 7).

Fluorescein isothiocyanate-lectin perfusion for assessment of transpial collaterals

To determine transpial collateralization across the EMS, an in vivo fluorescein isothiocyanate (FITC)-lectin perfusion was performed via the external carotid artery ipsilateral to the side of the EMS in two groups of animals with and without MCA-O (please see above). The ipsilateral external carotid artery was cannulated with a polyethylene catheter (inner diameter 0.28 mm; outer diameter 0.61 mm) connected to a micro syringe. The ipsilateral common carotid artery was proximally ligated, and a solution of 50 µl (100 µg) FITC-lycopersicon esculentum (tomato) lectin (Vector Laboratories Inc., Burlingame, CA, USA) and 200 µl phosphate-buffered saline was injected. The mice were decapitated within 2 s after the injection, and whole-head specimens were snap-frozen at −80 °C. To characterize the positive or negative development of transpial collaterals, we defined the *EMS take-rate* parameter: In each section, transpial collateralization was determined positive only after direct visual confirmation of (a) continuous FITC-lectin-positive vessels crossing from the muscle into the cortex and (b) a distinct association of these vessels with the resident vasculature of the cortical region below the EMS. The total number of sections with positive transpial collaterals was counted in each animal, and the individual EMS take-rate was defined positive if collaterals were noted in ≥50% of all section levels. The overall take-rate was calculated as the percentage of positive versus negative EMS. Further, correlation between the number of collaterals and CVRC was analyzed to assess the effect of transpial collateralization on the hemodynamic response (day 21: EV n = 5, VEGF n = 6, PDGF n = 6, VIP n = 6; day 42: EV n = 7; VEGF n = 7, PDGF n = 7, VIP n = 7; day 84: EV n = 6, VEGF n = 8, PDGF n = 6, VIP n = 7).

Immunohistochemistry

To assess fusion and reporter gene expression of implanted myoblasts at the muscle/brain interface of the EMS, an X-gal stain was performed on day 21 after implantation and is described elsewhere in detail.[28] Briefly, 60 µm coronal cryosections of snap-frozen, whole-head specimens were fixed with 4% paraformaldehyde, rinsed in phosphate-buffered saline and incubated with X-gal reaction buffer (diluted 40 mg/ml X-gal in dimethylformamide to 1:40 with X-gal dilution buffer) for 24 h. Myoblast fusion and reporter gene expression were identified according to the visual confirmation of β-gal positive cells.

For analysis of transpial collaterals and neuron survival after MCA-O, vessel density and pericyte coverage, proliferation and neuronal apoptosis, and astrocyte activation with VEGF or phospho-PDGF-Rβ co-localization, 10 µm coronal cryosections of snap-frozen, whole-head specimens were obtained from the anterior, middle and posterior region of the EMS (bregma −0.5 mm, −1.5 mm and −2.5 mm, respectively). Sections were mounted and visualized under a fluorescence-enhanced microscope (Axio Imager 2, Zeiss, Oberkochem, Germany). For analysis of pericyte recruitment of transpial collaterals, 20 µm cryosections were obtained in animals that underwent FITC-lection perfusion without MCA-O and visualized under a laser-scanning microscope (LSM710, Zeiss, Oberkochem, Germany). Negative control information was obtained by incubating tissue samples with only the corresponding secondary antibodies.

To determine surviving neurons following MCA-O together with patent transpial collaterals, NeuN-positive cells per mm^2 (days 21, 42 and 84) and FITC-lectin-positive collaterals per animal (day 42) were counted in the cortical region below and across the muscle/brain interface of the EMS (day 21: EV n = 5, VEGF n = 6, PDGF n = 6, VIP n = 6; day 42: EV n = 7; VEGF n = 7, PDGF n = 7, VIP n = 7; day 84: EV n = 6, VEGF n = 8, PDGF n = 6, VIP n = 7). To assess the morphology of transpial collaterals (EV n = 7, VEGF n = 7, PDGF n = 7, VIP n = 7) and the cortical vasculature (EV n = 4, VEGF n = 4, PDGF n = 4, VIP n = 4) on day 42, the vessel density and pericyte coverage were evaluated by a combined CD31/Desmin stain. Vessel density within the cortical area below the EMS was calculated as CD31-positive vessels per mm^2 for vessels below and above 10 µm in diameter. Pericyte coverage for the cortical vessels and transpial collaterals was expressed as the percentage of CD31-positive vessels with Desmin co-localization. Neuronal apoptosis on day 42 (EV n = 4, VEGF n = 4, PDGF n = 4, VIP n = 4) in the cortical region below the EMS was assessed by a combined TUNEL/NeuN stain. Apoptotic neurons were calculated as cells

per mm^2 (Supplemental Figure I). Astrocyte activation and VEGF or phospho-PDGF-Rβ co-localization in relationship to the cortical vasculature below the EMS on day 42 (EV n = 4, VEGF n = 4, PDGF n = 4, VIP n = 4) were detected by a combined glial fibrillary acidic protein (GFAP)/VEGF or phospho-PDGF-Rβ/CD31 stain. GFAP/VEGF or phospho-PDGF-Rβ co-localization was calculated as surface area (μm^2) per mm^2 or pPDGF-Rβ coverage (%) of the GFAP-positive surface area, respectively.

Surviving neurons were detected using mouse monoclonal anti-mouse NeuN (5 µg/ml, Millipore, Darmstadt, Germany) detected by Dylight 649-conjugated goat anti-mouse IgG antibody (1.25 µg/ml, BioLegend, San Diego, CA, USA). Vessel density and pericyte coverage were evaluated by a rat anti-mouse CD31 (0.31 µg/ml, BD Biosciences, Franklin Lakes, NJ, USA) detected by Cy3-conjugated donkey anti-rat IgG antibody (7.5 µg/ml, Jackson ImmunoResearch Laboratories, West Grove, PA, USA) and a rabbit anti-mouse Desmin (10 µg/ml, Abcam, Cambridge, UK) detected by Dylight 649-conjugated donkey anti-rabbit IgG antibody (1.25 µg/ml, BioLegend, San Diego, CA, USA). Neuronal apoptosis in the cortical region below the EMS was evaluated by TUNEL (Apoptosis detection kit, CHEMICON International Inc., Merck Life Science, Darmstadt, Germany) and NeuN co-localization. For assessment of astrocyte and VEGF co-localization in the cortical region below the EMS, GFAP was identified by a polyclonal chicken anti-GFAP (21.6 µg/ml, Abcam, Cambridge, UK) detected by fluorescein-conjugated goat anti-chicken IgY antibody (5 µg/ml, Abcam, Cambridge, UK). The VEGF expression on responsive astrocytes was visualized by a rabbit anti-VEGFA (10 µg/ml, Abcam, Cambridge, UK) detected by Cy3-conjugated anti-rabbit IgG antibody (5 µg/ml, Abcam, Cambridge, UK). The expression of phospho-PDGF-Rβ was visualized by a rabbit anti-phosphoY740 PDGF-Rβ (10 µg/ml, Abcam, Cambridge, UK) detected by Cy3-conjugated donkey anti-rabbit IgG antibody (7.5 µg/ml, Jackson ImmunoResearch Laboratories, West Grove, PA, USA).

Real-time PCR and Western blot

For analysis of exogenous (IRES) gene product transcription and VEGF/hPDGF-BB protein expression in the temporalis muscle and within the muscle/brain interface of the EMS on day 42, tissue samples of the temporalis muscle and the interface were harvested and snap-frozen for real-time PCR (rtPCR) and Western blot analysis (EV n = 4, VEGF n = 4, PDGF n = 4, VIP n = 4).

For transcription analysis, RNA isolation was performed with Trizol, according to standard Trizol extraction protocol (Invitrogen, Carlsbad, CA, USA). The amount of RNA was quantified using Infinite 200 PRO (TECAN, Männedorf, Switzerland). cDNA was reversely transcribed using QuantiTec Reverse Transcription Kit (Qiagen, Venlo, Netherlands) according to the manufacturer's recommendation. Real-time PCR amplifications were performed in triplicates in a 25 µl reaction volume using the SYBR Premix Ex Taq Kit (Takara Bio Inc., Shiga, Japan) with the indicated primer pairs of IRES-forward: GC TCTCCTCAAGCGTATTCAACA and IRES-reverse: CCCCAGATCAGATCCCATACA and a 7900HT Fast rtPCR System or ABI Prism 7000 Sequence Detection System (Applied Biosystems, Foster City, CA, USA). For standardization, GAPDH was used as housekeeping gene (GAPDH-forward: GGCCTT CCGTGTTCCTACC; GAPDH-reverse: AACCTG GTCCTCAGTGTACC). All data were analyzed by the relative quantification method (ΔΔCt). For Western blot, samples harvested from the temporalis muscle or the muscle/brain interface were homogenized with a solution of RIPA buffer and protease inhibitors (ratio Sample:RIPA = 1:10). For Western blot analysis, the protein concentration of each sample was determined using a Pierce BCA Protein Assay Kit (Thermo Fisher Scientific, Waltham, MA, USA) according to the standard protocol. Samples containing 100 µg of protein were subjected to 10% polyacrylamide gel electrophoresis in the presence of 0.1% sodium dodecyl sulfate. Protein bands were transferred from the gel to PVDF membranes, which were incubated with a 1:1000 dilution of rabbit polyclonal anti-VEGFA antibody (1 µg/ml, Abcam AB46154, Cambridge, UK) or with 1:100 dilution of rabbit polyclonal anti-PDGF antibody (1 µg/ml, Abcam AB16829, Cambridge, UK), and membranes were reacted with horseradish peroxidase-conjugated donkey anti-rabbit IgG antibody (Jackson ImmunoResearch Laboratories, West Grove, PA, USA). Protein bands on membranes were detected by an enhanced chemiluminescence method. Quantification of the Western Blot bands was performed after normalization of the GAPDH densities. First, images were converted to 8bit grayscale, and identical threshold intensity settings were applied with the help of image processing and analysis software (ImageJ, Ver. 2.0.0-rc-68/1.52g, https://imagej.nih.gov/ij/). Next, we determined the background-subtracted densities (Integrated Density) of the protein of interest (PI; VEGF or PDGF-BB) and the normalizing control (GAPDH) bands. For each PI, we then identified the GAPDH band with the highest density (Control, VEGF, PDGF or VIP). In order to obtain a normalized GAPDH value, we then divided all GAPDH density values by the highest GAPDH density value. To then quantify the density of

the PI in each lane based on the normalized GAPDH value, each PI density was divided by the normalized GAPDH value in their respective lane.

Statistical analysis

Data are presented as mean ± standard deviation (SD) or percentage. All continuous variables passed normality and equal variance testing, determined by the Shapiro-Wilks and F-Test, and parametric testing was performed accordingly. Baseline perfusion and CVRC were compared by a two-way ANOVA for repeated measurements with subsequent pair-wise comparison of means by Fisher's least projected difference test. Cortical infarct size, NeuN-positive cells after MCA-O, transpial collaterals, EMS take rate, vessel density, pericyte coverages, neuronal apoptosis and GFAP/VEGF or phospho-PDGF-Rβ co-localization were compared by a one-way ANOVA procedure with Bonferroni correction for multiple comparisons. Relative quantity (ΔΔCt) using IRES primer in real-time PCR was compared by a non-parametric Kruskal-Wallis test with Dunn's post hoc analysis for multiple comparisons. For correlation of "Cortical infarction" versus "CVRC" and "Number of collaterals" versus "CVRC," a Spearman correlation analysis was used due to failed normality tests. Statistics were performed with GraphPad Prism for Mac (Version 5.0f, GraphPad Software, San Diego, California, USA). Statistical significance was set at $p<0.05$.

Results

Myoblast engraftment and gene product expression

On day 21, X-gal staining revealed successfully fused hybrid myofibers in all experimental groups (Figure 1(a)). A blush extracellular β-gal signal as a sign of local reporter gene expression by non-fused myoblasts without fiber structure was noted particularly after implantation of PGDF myoblasts. In the temporalis muscle, rtPCR using IRES primer on day 42 confirmed the exogenous transcription of $VEGF_{164}$ and/or hPDGF-BB in VEGF-, PDGF- and VIP-myoblasts, respectively, with the highest transcription rate noted in PDGF myoblasts. An increased amount of total VEGF and/or hPDGF-BB in the temporalis muscle following implantation of VEGF-, PDGF- or VIP myoblasts was confirmed by Western blot (Figure 1(b)).

Hemodynamic rescue following $VEGF_{164}$ and hPDGF-BB co-delivery

Laser Speckle Images of typical resting perfusion and cortical blood flow responses to acetazolamide on day 42 are illustrated in Figure 2 and expressed as

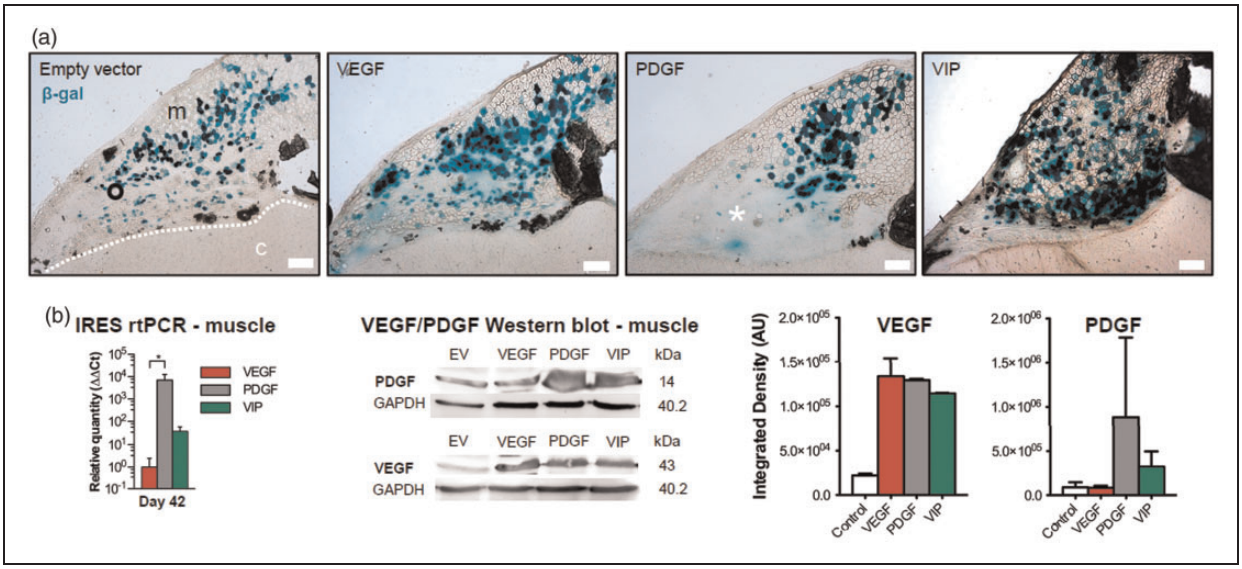

Figure 1. Myoblast engraftment and gene-product expression. (a) Immunohistochemical X-gal staining confirms stable engraftment of EV, VEGF, PDGF and VIP myoblasts on day 21 after implantation into the temporalis muscle. The asterisk within the area of blush reporter gene expression exemplifies a local tumor formation after implantation of myoblasts expressing hPDGF-BB alone. Bar = 200 μm; m: muscle; c: cortex; dashed line: muscle/brain interface. (b) Real-time PCR using IRES primer and Western blot confirm exogenous gene product transcription and protein expression within the temporalis muscle on day 42 after myoblast implantation; *$p<0.05$. The panels on the right show the normalized integrated densities corresponding to the Western Blot bands for VEGF and PDGF-BB.

VEGF: vascular endothelial growth factor; PDGF: platelet-derived growth factor; IRES: internal ribosomal entry site.

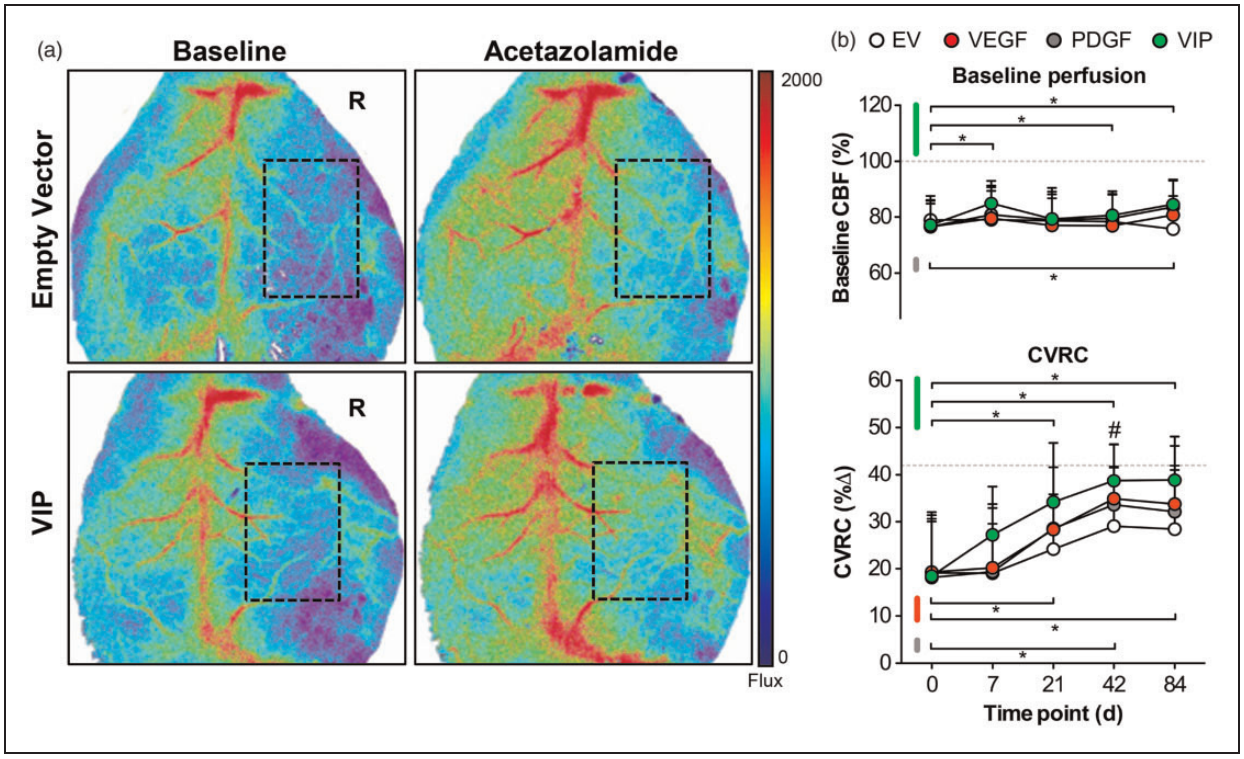

Figure 2. Hemodynamic rescue following VEGF164 and hPDGF-BB co-delivery. (a) Real-time laser speckle images of cortical perfusion before (left) and after (right) acetazolamide showing the improved hemodynamic response in VIP-treated animals on day 42. The dashed rectangle shows the area of perfusion assessment. R: right. (B) Line graphs illustrating the mean resting (baseline) perfusion (CBF-Flux; upper panel) and mean cerebrovascular reserve capacity (CVRC expressed as the percent change in CBF-Flux; lower panel) in animals treated with EV, VEGF, PDGF or VIP myoblasts over the 84-day monitoring period. Although baseline perfusion (upper panel) remained stable during the monitoring period, statistical differences compared to day 0 were found on days 7, 21 and 84 in VIP-treated animals and on day 84 in animals that received PDGF myoblasts (*$p<0.05$ versus day 0 for VIP and PDGF). Regarding hemodynamic recovery, however, VIP resulted in superior hemodynamic rescue compared to day 0 beginning at day 21 (*$p<0.05$), next to significant CVRC improvement on day 42 compared to empty vector (EV) myoblasts (#$p<0.05$ for VIP vs. EV). To a lesser extent, hemodynamic rescue compared to day 0 was also noted in VEGF and PDGF-treated animals (*$p<0.05$ compared to day 0 for VEGF and PDGF). The dashed horizontal lines illustrate the normalized resting perfusion (100%) and mean CVRC (42%) of the non-occluded hemispheres on day 0.

EV: empty vector; VEGF: vascular endothelial growth factor; PDGF: platelet-derived growth factor; CVRC: cerebrovascular reserve capacity; CBF: cerebral blood flow.

percentage compared to contralateral (resting perfusion) or overall percentage (CVRC). First, we analyzed resting (baseline) perfusion between treatment groups. On day 0 following ICA-O with EMS and myoblast implantation, resting perfusion over the affected hemisphere was reduced >20% and comparable between groups. Although none of the groups reached resting perfusion levels of the contralateral hemisphere, animals treated with VIP myoblasts showed signs of a sustained perfusion increase over time (Figure 2(a) and (b), upper panel). We then focused on the cortical perfusion response after acetazolamide challenge: Compared to the hemodynamic response over the unaffected hemisphere on day 0, CVRC over the affected hemisphere on day 0 was reduced > 50% and comparable between groups. Over time, spontaneous hemodynamic rescue occurred in all groups with the earliest and most pronounced CVRC recovery in VIP-treated animals, followed by animals treated with VEGF-myoblasts (Figure 2(a) and 2(b), lower panel).

Cortical stroke and regional perfusion following MCA-O

At day 42, animals treated with VIP myoblasts had a 30–35% reduction of cortical infarction compared to animals treated with PDGF or EV myoblasts. At day 84, this benefit for VIP- compared to EV-treated animals was sustained, corresponding to a 38% reduction of cortical T2 signal hyperintensity. LSI confirmed sustained cortical perfusion during the MCA-occlusion period in VIP-treated animals compared to animals that only received EV myoblasts. A significant negative correlation was found between the percentage of

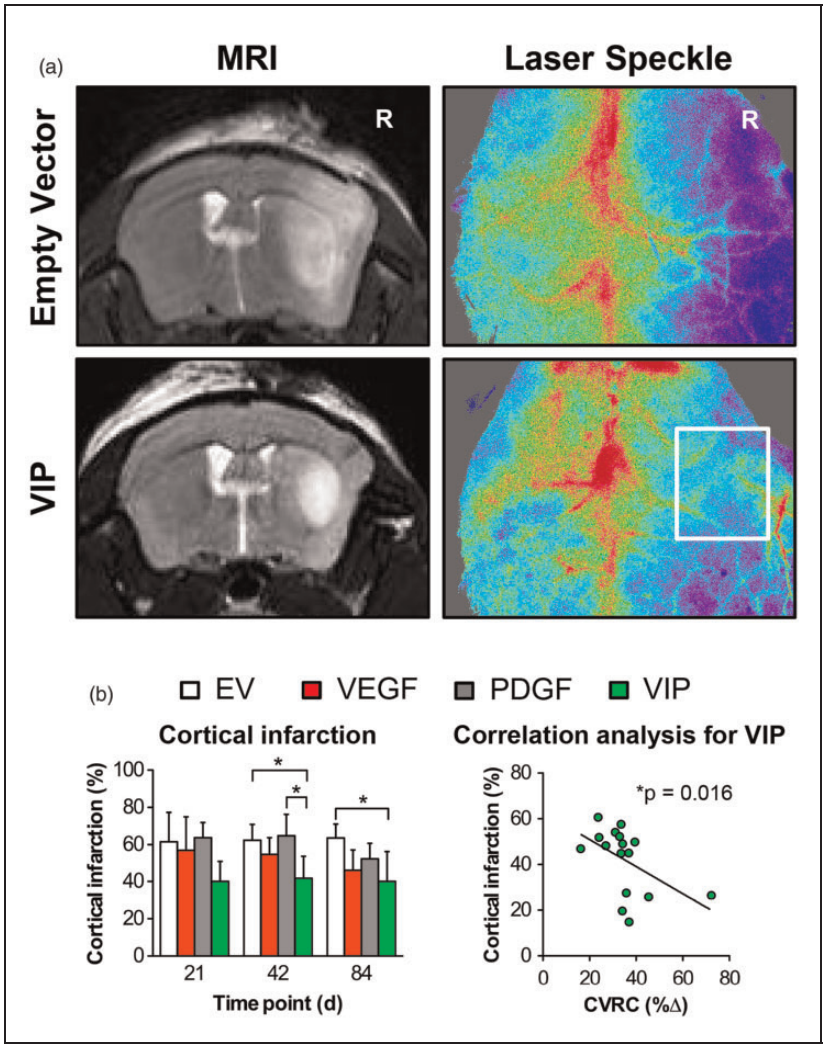

Figure 3. Cortical stroke and regional perfusion following MCA-O. (a) T2-weighted MR (left) and laser speckle (right) images illustrating the differences in T2 signal hyperintensity (defined as infarction) and perfusion after ipsilateral MCA-O on day 42 in animals treated with EV (upper panels) and VIP (lower panels) myoblasts. R: right. (b) Bar graph illustrating the percentage of cortical infarction (*$p<0.05$) determined in MR imaging and correlation analysis confirming the significant association between the size of the infarction and the degree of hemodynamic impairment in VIP-treated animals (*$p=0.016$; $r=-0.59$).
EV: empty vector; VEGF: vascular endothelial growth factor; PDGF: platelet-derived growth factor; CVRC: cerebrovascular reserve capacity; CBF: cerebral blood flow.

cortical infarction and the degree of hemodynamic impairment (*$p=0.016$; $r=-0.59$) (Figure 3).

Neuroprotection after MCA-O and transpial collateralization

Following proximal stroke through MCA-O at day 21, 42 and 84, VIP-treated animals had a significantly higher number of surviving neurons in the cortical region below the EMS than animals treated with EV myoblasts alone (Figure 4(a) and (b)). On day 42, positive spontaneous transpial collateralization was detected in all groups with an 85% increase in patent extra- to intracranial collaterals and the highest EMS take-rate in VIP-treated animals compared to animals that received EV myoblasts (Figure 4(c)). The functional hemodynamic relevance of this improved collateralization is suggested by a significant correlation of the number of collaterals to the CVRC (**$p=0.0076$; $r=0.29$), next to the 20% greater relative CVRC difference in animals with 10 or more collaterals (Figure 4(d)).

Vessel density, pericyte recruitment and neuronal apoptosis

At day 42, treatment with VIP and PDGF myoblasts resulted in a significant 50% increase in the density of cortical vessels $>10\,\mu m$ compared to animals that only

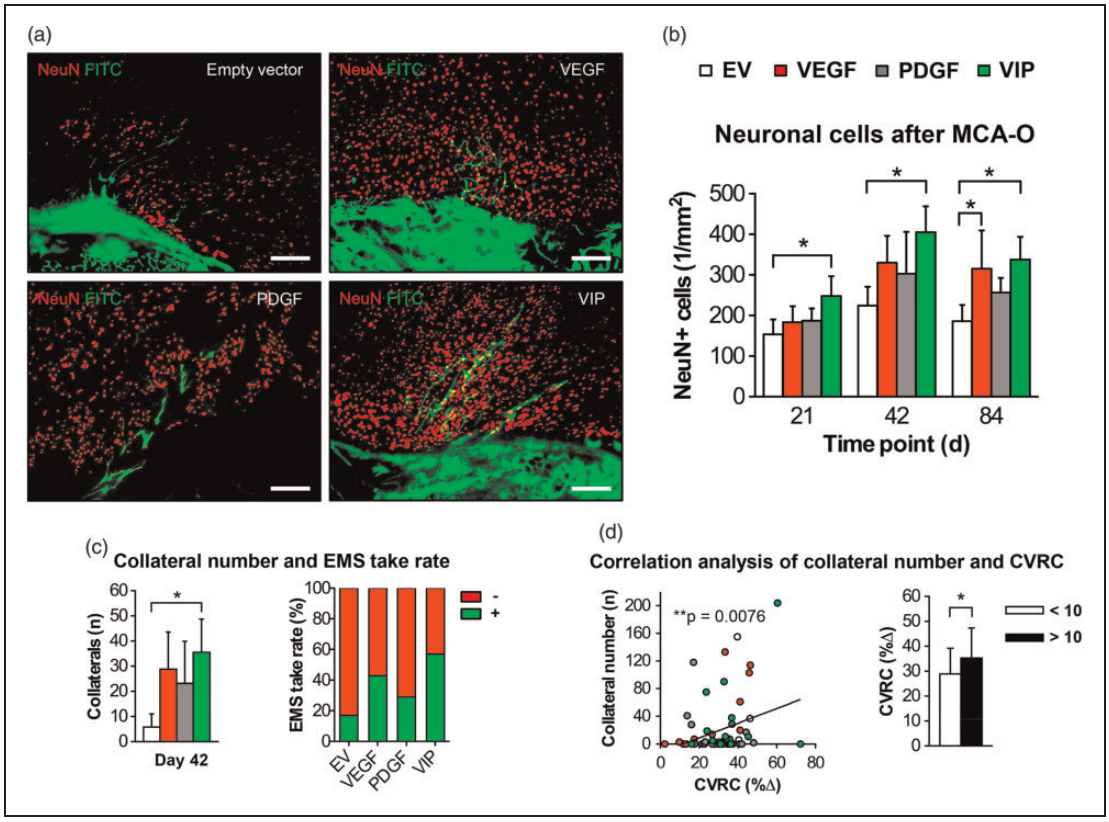

Figure 4. Neuroprotection after MCA-O and transpial collateralization. (a) Photomicrographs of the muscle/brain interface after MCA-O and FITC-lectin perfusion on day 42 illustrating the higher number of surviving neuronal cells post stroke together with the increased EMS collateralization measured as the number of transpial collaterals in VIP-treated animals. Bar = 100 μm. (b) Bar graph illustrating the number of NeuN-positive cells in the cortical region below the EMS (*$p<0.05$) and (c) showing the corresponding number of transpial collaterals (left) and the EMS take-rate (right) determined by FITC-lectin perfusion through the external carotid artery feeding the EMS after ipsilateral MCA-O; *$p<0.05$. (d) Correlation analysis between the degree of hemodynamic impairment and the number of transpial collaterals on day 42 (**$p = 0.0076$; $r = 0.29$). The bar graph illustrates the CVRC depending on the number of collaterals; *$p<0.05$.

EV: empty vector; VEGF: vascular endothelial growth factor; PDGF: platelet-derived growth factor; CVRC: cerebrovascular reserve capacity; CBF: cerebral blood flow; FITC: fluorescein isothiocyanate; EMS: encephalomyosynangiosis; MCA-O: middle cerebral artery-occlusion.

received EV myoblasts, which was paralleled by a 13–15% increase in pericyte coverage of vessels <10 μm, indicating an increased microvascular maturation (Figure 5(a) and (b)). Regarding the morphology of transpial collaterals, however, only VIP-treated animals consistently showed a dense mural Desmin coverage of the FITC-positive extra- to intracranial collaterals crossing from the muscle into the brain (Figure 5(c) and (d)). Further, TUNEL staining on day 42 revealed an 85% reduction of apoptotic neurons following treatment with VIP compared to EV myoblasts (Supplemental Figure I).

PDGF-BB dependent astrocyte activation with intrinsic VEGF mobilization

In addition to its role in stimulating vessel growth and maturation, VEGF and PDGF-BB are important neurotrophic factors that have the potential to enhance the neurogenic capacity in the brain through astrocytic activation, which is morphologically characterized by hypertrophy of astrocytic somata, processes and prominent expression of GFAP.[32–34] Also, VEGF and its receptors are expressed in astrocytes themselves and the level of intrinsic VEGF is upregulated upon astrocytic activation.[35] As a last step, we therefore investigated direct effects of local growth factor supplementation on astrocytes below the EMS. Here, GFAP immunofluorescence suggested an increased astrocytic activation in the cortical region below the EMS after PDGF- and VIP-myoblast implantation. Particularly in animals that received a balanced co-delivery of hPDGF-BB and $VEGF_{164}$, activated astrocytes were in direct contact with CD31-positive parenchymal vessels and showed significant VEGF

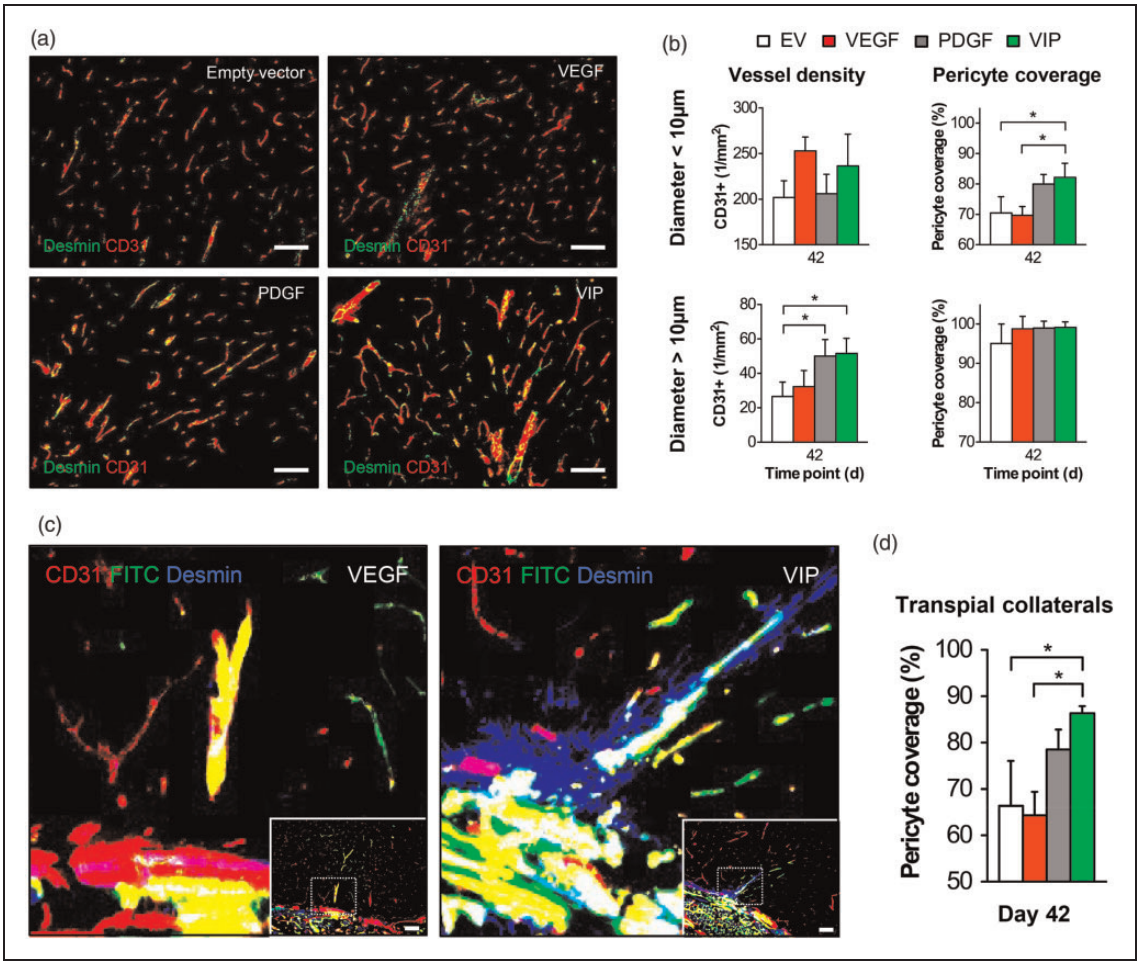

Figure 5. Vessel density and pericyte recruitment. (a) Photomicrographs of the cortical region below the EMS on day 42 showing the increased CD31-positive signal and CD31/Desmin co-localization following EMS and implantation of VIP myoblasts. Bar = 100 μm. (b) Bar graphs of the microvascular density (1/mm^2) and vascular pericyte coverage (%) in vessels < 10 μm (upper graphs) and > 10 μm (right); *p<0.05. (c) High-power magnification photomicrographs of the muscle/brain interface obtained with confocal imaging in animals that underwent FITC-lectin perfusion for visualization of transpial collaterals in combination with CD31/Desmin staining illustrate the increased pericyte recruitment around patent transpial collaterals as a distinct peri-collateral Desmin-positive signal in animals that received VIP. The dashed rectangle illustrates the area of detail enlargement. Bar = 100 μm. (d) Bar graph quantifying the pericyte coverage of transpial collaterals; *p<0.05.
EV: empty vector; VEGF: vascular endothelial growth factor; PDGF: platelet-derived growth factor.

co-localization, possibly due to increased intrinsic VEGF mobilization upon astrocytic activation (Figure 6(a) and (b)). X-gal staining, rtPCR and Western blot analysis confirmed positive reporter gene expression, gene product transcription and increased VEGF and/or hPDGF-BB levels at the muscle/brain interface of the EMS on day 42 (Figure 6(c) and (d)). Next to increased astrocytic activation, we found a marked elevation of phospho-PDGF-Rβ signal intensity in the cortical region of the EMS together with a significantly higher co-localization of phospho-PDGF-Rβ and the GFAP-positive surface area (Figure 7).

Discussion

In the present model of chronic cerebral ischemia and EMS, co-delivery of VEGF and PDGF-BB led to superior EMS collateralization and hemodynamic rescue with increased ischemic protection compared to delivery of VEGF or PDGF-BB alone. Improved vascular maturity was a key factor associated with these beneficial effects. Further, our findings suggest that PDGF-BB-mediated astrocytic activation might serve as a secondary neuroprotective mechanism independent from therapeutic collateralization.

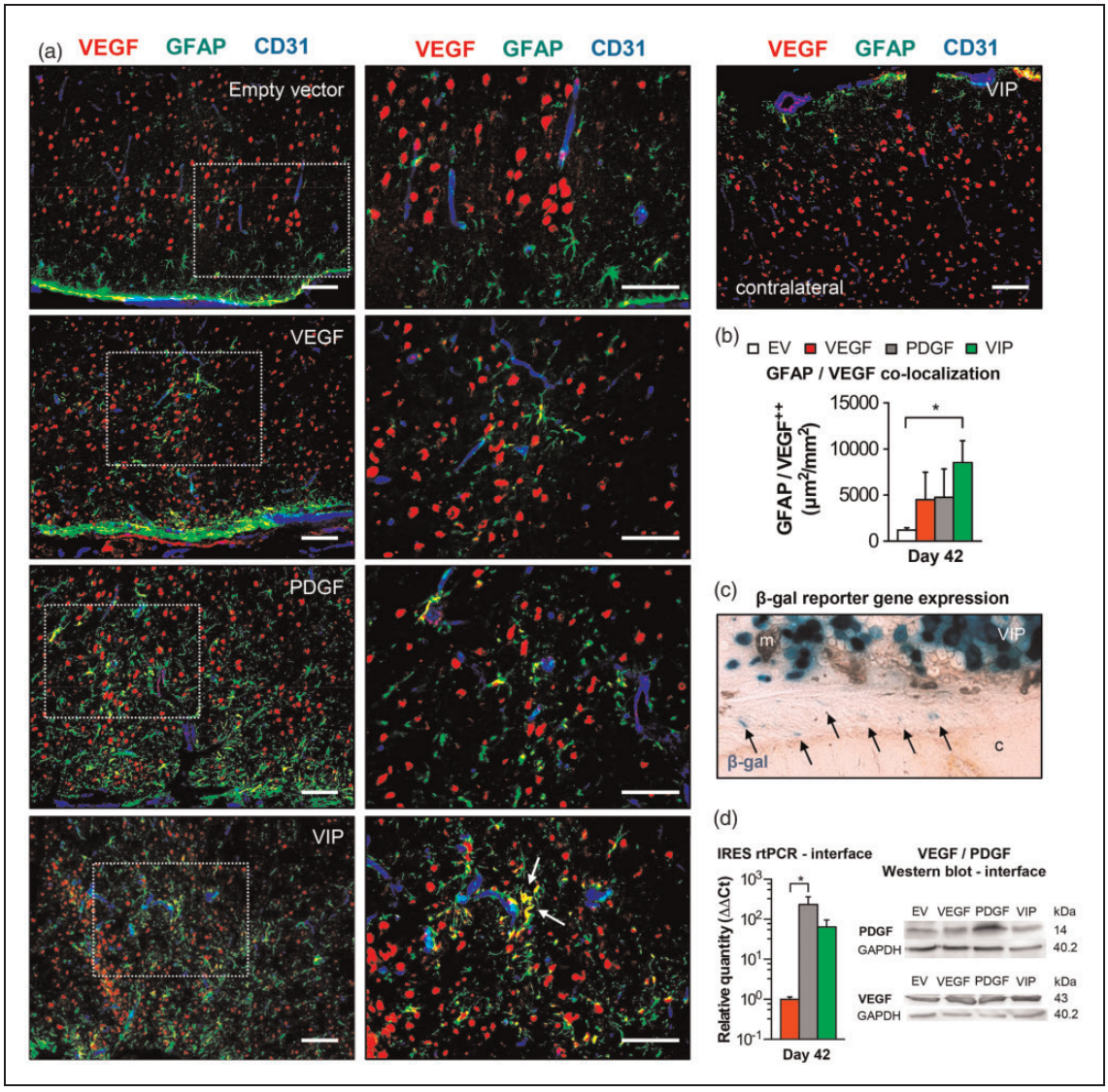

Figure 6. Astrocyte activation and intrinsic VEGF mobilization. (a) Photomicrographs of the cortical region below the EMS and of an untreated hemisphere on day 42 showing increased GFAP-positive astrocytic activation in animals receiving PDGF or VIP myoblasts with GFAP/VEGF co-localization (arrows) as a sign of intrinsic VEGF mobilization in VIP-treated animals. The dashed rectangle identifies the area of detail enlargement on the right. Bar = 100 µm. (b) Bar graph quantifying the area (μm^2) of GFAP/VEGF co-localization per mm^2; *$p<0.05$. (c) Reporter gene expression at the muscle/brain interface (arrows) and (d) real-time PCR using IRES primer and Western blot confirm exogenous gene product transcription and protein expression at the muscle/brain interface on day 42 after myoblast implantation; *$p<0.05$. m: muscle; c: cortex.
EV: empty vector; VEGF: vascular endothelial growth factor; PDGF: platelet-derived growth factor; GFAP: glial fibrillary acidic protein.

Growth factor expression and myoblast engraftment

VEGF is a critical mediator of cerebral collateral development and maintenance in the adult mouse brain.[13,14,16,29] However, VEGF-induced neovascularization requires increased levels of VEGF to achieve beneficial effects, yet high VEGF expression levels readily lead to a loss of safety. In the present study, $VEGF_{164}$ alone was delivered at its most optimal microenvironmental dose by a monoclonal myoblast population homogeneously expressing the most therapeutic amount of $VEGF_{164}$, as determined previously.[17,18] In comparison, co-delivery of $VEGF_{164}$ and hPDGF-BB at a fixed ratio was enacted without any kind of dose control. This co-expression through the VIP construct previously enabled robust VEGF delivery and further expanded the functional efficacy of VEGF alone.[25] Regarding engraftment, we were

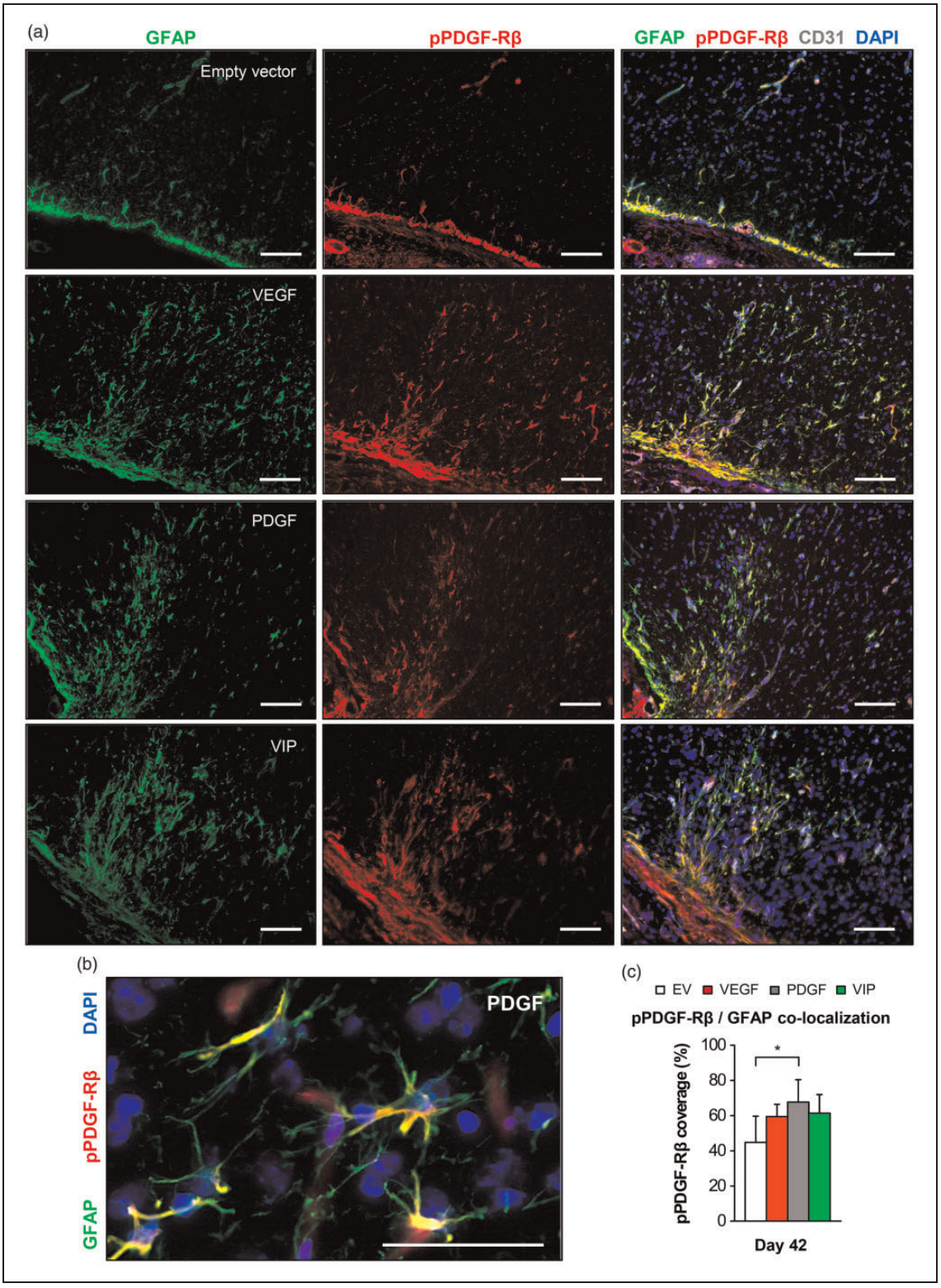

Figure 7. Phospho-PDGF-Rβ/GFAP co-localization in the cortical region below the EMS. (a) Photomicrographs of the cortical region below the EMS on day 42 showing an increased GFAP-positive signal in animals receiving VEGF, PDGF or VIP myoblasts together with marked phospho-PDGF-Rβ expression. Bar = 100 μm. (b) High-power magnification showing astrocytic GFAP/phospho-PDGF-Rβ co-localization. Bar = 50 μm. (c) Quantification of the percent phospho-PDGF-Rβ-coverage of the GFAP-positive surface area; *$p<0.05$. EV: empty vector; VEGF: vascular endothelial growth factor; PDGF: platelet-derived growth factor; GFAP: glial fibrillary acidic protein.

able to confirm stable fusion and gene product expression of all implanted myoblast populations within the temporalis muscle of the EMS. The different transcription levels that we observed within the muscle and at the muscle/brain interface are likely associated with the fact that PDGF and VIP myoblasts tend to engraft better than the remaining myoblast populations due to the trophic effects of hPDGF-BB on the myoblasts themselves. Interestingly, in some cases, PDGF myoblasts resulted in local tumor development within the temporalis muscle, as indicated in Figure 1(a). Most likely, this is caused by excessive hPDGF-BB expression by some of the myoblasts in the polyclonal population due to random differences in copy number and genomic integration sites of the retroviral vector. The blush β-gal signal instead of a fiber structure indicates that such tumors are not formed exclusively by the myoblasts, which actually encounter an unfavorable environment for differentiation and remain as single cells.

Hemodynamic rescue, transpial collateralization and ischemic neuroprotection

In clinical practice, the degree of cerebrovascular reactivity remains the most important parameter to assess the patients' risk of hemodynamic ischemic stroke, because non-ischemic cerebral hypoperfusion is typically characterized by a normal or at best only mild reduction of baseline (resting) perfusion.[2] Therefore, we first addressed whether $VEGF_{164}$ and hPDGF-BB co-expression at the muscle/brain interface of an EMS translated into improved cerebral hemodynamics. In this regard, only VIP-treated animals experienced nearly complete hemodynamic rescue, whereas the CVRC in animals treated with EV, VEGF or PDGF myoblasts alone remained 30–15% below the CVRC response of the non-occluded hemisphere. The time line of this hemodynamic rescue was in line with our present and previous results regarding the time points of myoblast host integration, collateral outgrowth and vascular remodeling.[17,18,23,29] Importantly, the improved hemodynamics following VIP treatment were not accompanied by an overshooting CVRC response or perfusion increase, which is essential to avoid critical postoperative hyperperfusion in hemodynamically compromised patients undergoing surgical revascularization.[36]

The main goal of an EMS is the reduction of subsequent ischemic events through improvement of collateral flow at the level of the leptomeningeal vasculature, which is a major determinant in the severity of stroke.[37] Therefore, we next tested whether our hemodynamic findings also translated into improved collateralization and regional ischemic protection: Indeed, only treatment with VIP myoblasts resulted in a significant and sustained 38% reduction of cortical infarct volume after proximal MCA-O, together with a significantly greater number of patent transpial collaterals. For the first time, we were also able to show a direct link between the size of cortical infarction, the degree of transpial collateralization and the degree of hemodynamic CVRC impairment, which correlated not only with the percentage of cortical infarction but also with the number of transpial collaterals. The reason for focusing on cortical instead of subcortical infarction is the variable degree of native basal and leptomeningeal collateralization in C57BL/6 mice, which results in highly variable subcortical stroke volumes after MCA filament occlusion.[38,39] In the setting of chronic cerebral ischemia, we were able to confirm our previous findings that an experimental EMS mainly provides ischemic protection in the cortical territories surrounding the newly formed transpial collaterals.[29] Since the proportional volume of the cerebral cortex is much smaller than that of the subcortical region, additional analysis of the subcortical stroke volume in our model would mask the protective effect of the EMS. On the other hand, a distal MCA-O model with only a localized focal cortical stroke was not feasible due to the adhesive EMS, which limits access to the leptomeningeal cerebral vasculature without injuring the transpial collaterals. This relationship between improved EMS collateralization and greater ischemic protection is verified by the sustained cortical perfusion across the EMS during MCA-O and in line with our observed neuroprotection under myoblast-mediated co-delivery of $VEGF_{164}$ and hPDGF-BB.

Vascular maturation and pericyte recruitment

While VEGF is the crucial factor to promote endothelial cell growth, PDGF-BB is essential for stabilization of blood vessels by recruiting pericytes for regulation of vessel diameters and blood flow.[20,21] However, VEGF may also act as a negative regulator of pericyte function and vessel maturation,[19] which is suggested by the fact that $VEGF_{164}$ alone failed to sustain pericyte recruitment around parenchymal microvessels or transpial collaterals. In comparison, treatment with $VEGF_{164}$ and hPDGF-BB co-expressing VIP myoblasts not only resulted in improved hemodynamic rescue, transpial collateralization and ischemic protection but also in a higher pro-angiogenic activity with significantly improved pericyte recruitment as a sign of greater vascular maturation. Remarkably, this increased pericyte recruitment was also noted around the newly formed transpial EMS collaterals and paralleled by an activation of PDGF receptor beta (PDGF-Rβ) (Supplemental Figure II), which may have relevant clinical implications, because autopsy reports in patients that underwent an EMS demonstrated that the

transpial EMS collaterals appear to have a fragile structure with a thin and sparse media composed mainly of smooth muscle actins without a mature perivascular network.[40] Also, we cannot exclude that an increased microvascular smooth muscle cell coverage and subcortical capillary arterialization, where remodeled capillaries function as collaterals to hypoperfused tissue, may have contributed to the hemodynamic rescue and ischemic protection that we noted.[13,14,31,41]

Direct effect and limitations of localized hPDGF-BB delivery

The sporadic tumor formation following implantation of polyclonal PDGF myoblasts requires a discussion of safety implications and their possible solutions: As stated, hPDGF-BB production by polyclonal PDGF myoblasts was almost five-fold higher than that of VIP myoblasts, which explains why tumors were not observed in the VIP-treated animals. Further, our work provides proof-of-principle of the superiority of the combination delivery over VEGF delivery alone, even if VEGF is delivered in its most optimal, homogeneous dose by the monoclonal population employed here. However, refinements need to be enacted for therapeutic application, such as rapid FACS purification to exclude cells expressing excessive PDGF-BB doses, which can easily be performed based on the intensity of the CD8 marker, as described previously.[42] The sporadic tumor formation following hPDGF-BB supplementation also explains another surprising observation: In contrast to what might have been expected, we noted a similar hemodynamic recovery following hPDGF-BB supplementation and supplementation of $VEGF_{164}$ alone, which could be due to the high amount of VEGF protein also in hPDGF-BB-treated groups. This anomalous amount of VEGF protein in tissue treated with PDGF myoblasts is most likely endogenous and upregulated due to tumor formation with ensuing hypoxia, which functionally causes the tissue treated with PDGF myoblasts to behave like tissue under VEGF conditions. Nevertheless, co-delivery of $VEGF_{164}$ and hPDGF-BB in VIP myoblasts still remained superior, because the expression of both factors is balanced and coordinated through the bi-cistronic VIP vector in every cell, whereas in hPDGF-BB-induced tumors, both factors are expressed heterogeneously throughout the tissue. Although we did not find significant differences of the endogenous $VEGF_{164}$ expression within the temporalis muscle, transcription of endogenous $VEGF_{164}$ at the muscle/brain interface was significantly upregulated in VIP animals as sign of the increased pro-angiogenic activity in this group. Interestingly, we also noted a trend towards a higher endogenous $VEGF_{164}$ transcription in animals that received hPDGF-BB alone, which is in line with our hypothesis of tumor-ensuing hypoxia as a cause for the increased $VEGF_{164}$ protein levels in these animals (Supplemental Figure III).

Interestingly, myoblast-mediated growth factor supplementation also resulted in an increased activation of astrocytes and co-localization of VEGF within astrocytes/astrocytic processes and endothelial cells in the cortical parenchyma below the EMS (Figure 6 and Supplemental Figure IV). The significantly increased PDGF-Rβ expression on reactive astrocytes particularly in PDGF-treated animals (Figure 7) suggests that the observed astrocytic activation appears to be a direct effect following PDGF-BB delivery, which is in line with our reporter-gene expression analysis and molecular findings at the muscle/brain interface of the EMS but also with previous results, demonstrating a PDGF-BB-dependent astrocytic activation and pro-inflammatory response with monocyte recruitment via induction of monocyte chemoattractant protein 1 (MCP-1) and downstream activation of nuclear factor κB (NFκB).[17,18,23,29] Possibly, this astrocytic activation could be a second reason for favorable hemodynamic recovery, because activation of NFκB with stabilization of HIF-1α expression has been identified as a key pathway for capillary arterialization and maturation of a new arterial collateral network following shear stress-induced endothelial activation of collateral outgrowth.[16] Further, astrocytic activation could also have contributed to direct neuroprotection by reduction of reactive oxidant species and activation of antioxidant mechanisms within activated astrocytes[43] next to an increased intrinsic VEGF mobilization, which was shown to directly contribute to structural neuroprotection with improved functional recovery following acute ischemic stroke.[44,45] Apart from extracellular secretion, the pattern and shape of VEGF localization in GFAP- and CD31-negative areas could be an expression of nuclear and perinuclear VEGF accumulation in neuronal or peri-arteriole smooth muscle cells following the increase of HIF-1α expression as an adaptive change underlying a low oxygen environment in chronic hypoxia.[46,47]

Study design limitations

The use of only young, healthy, male animals requires explanation, because in preclinical stroke research internal and external validity must be reduced by limiting bias and including aged, co-morbid animals of both sexes. However, our present study was an exploratory proof-of-concept investigation with focus on a novel approach for therapeutic cerebral collateralization in a model of cerebral hypoperfusion, which we previously established in male C57BL/6N mice.[31] Importantly, the degree of chronic cerebral ischemia above the threshold of ischemic stroke in mice is largely influenced by

the native cerebral collateral vasculature, which underlies a high developmental variability and influences the degree of hemodynamic impairment.[31,38] Further, differences in molecular mechanisms of ischemic cell death and stroke outcome have been observed in males and females. This difference is usually assigned to the estrus cycle in female mice, because estrogen has been shown to protect the brain in numerous models of experimental brain injury. For the purpose of standardization, we therefore deliberately matched age, sex and genetic background of our animals according to our previously established model[29,31] and designed our experiments according to the initial Stroke Therapy Academic Industry Roundtable (STAIR) recommendations, where such exploratory studies are recommended to be performed in young, healthy animals without vascular disease or vascular risk factors.[48] Thus, to what extent the present approach would be beneficial if one of the driving risk factors for stroke and stroke outcomes were present still needs to be determined.

Authors' contributions

PV and NH contributed equally to this article. NH, PV and AB conceived, designed and supervised the trial. AM, MN, IK, JW, GvD and RG-B obtained and analyzed the data. AM and NH wrote the first draft of the article. All authors were involved in interpretation of the data and critical revision of the article and approved the final report.

Funding

The author(s) disclosed receipt of the following financial support for the research, authorship, and/or publication of this article: The Federal Ministry of Education and Research (BMBF), Center for Stroke-research Berlin (CSB) and by grants from the Deutsche Forschungsgemeinschaft (DFG: VA 244/10-1) FOR 2325 NVI.

Declaration of conflicting interests

The author(s) declared no potential conflicts of interest with respect to the research, authorship, and/or publication of this article.

ORCID iD

Andrea Banfi http://orcid.org/0000-0001-5737-8811

Supplemental material

Supplemental material for this paper can be found at the journal website: http://journals.sagepub.com/home/jcb

References

1. Powers WJ, Clarke WR, Grubb RL, et al. Extracranial-intracranial bypass surgery for stroke prevention in hemodynamic cerebral ischemia: the Carotid Occlusion Surgery Study randomized trial. *JAMA* 2011; 306: 1983–1992.
2. Grubb RLJ, Derdeyn CP, Fritsch SM, et al. Importance of hemodynamic factors in the prognosis of symptomatic carotid occlusion. *JAMA* 1998; 280: 1055–1060.
3. Amin-Hanjani S, Barker FG, Charbel FT, et al. Extracranial-intracranial bypass for stroke-is this the end of the line or a bump in the road? *Neurosurgery* 2012; 71: 557–561.
4. Kredel FE. Collateral cerebral circulation by muscle graft: technique of operation with report of 3 cases. *Southern Surgeon* 1942; 10: 235–244.
5. Karasawa J, Kikuchi H, Furuse S, et al. A surgical treatment of "moyamoya" disease 'encephalo-myo synangiosis'. *Neurol Med Chir (Tokyo)* 1977; 17: 29–37.
6. Czabanka M, Pena-Tapia P, Scharf J, et al. Characterization of direct and indirect cerebral revascularization for the treatment of European patients with moyamoya disease. *Cerebrovasc Dis* 2011; 32: 361–369.
7. Guzman R, Lee M, Achrol A, et al. Clinical outcome after 450 revascularization procedures for moyamoya disease. Clinical article. *J Neurosurg* 2009; 111: 927–935.
8. Kim S-K, Cho B-K, Phi JH, et al. Pediatric moyamoya disease: an analysis of 410 consecutive cases. *Ann Neurol* 2010; 68: 92–101.
9. Rafat N, Beck G, Pena-Tapia PG, et al. Increased levels of circulating endothelial progenitor cells in patients with moyamoya disease. *Stroke* 2009; 40: 432–438.
10. Blecharz KG, Frey D, Schenkel T, et al. Autocrine release of angiopoietin-2 mediates cerebrovascular disintegration in moyamoya disease. *J Cereb Blood Flow Metab* 2017; 37: 1527–1539.
11. Komotar RJ, Starke RM, Otten ML, et al. The role of indirect extracranial-intracranial bypass in the treatment of symptomatic intracranial atheroocclusive disease. *J Neurosurg* 2009; 110: 896–904.
12. Czabanka M, Vajkoczy P, Schmiedek P, et al. Age-dependent revascularization patterns in the treatment of moyamoya disease in a European patient population. *Neurosurg Focus* 2009; 26: E9.
13. Lucitti JL, Mackey JK, Morrison JC, et al. Formation of the collateral circulation is regulated by vascular endothelial growth factor-A and a disintegrin and metalloprotease family members 10 and 17. *Circ Res* 2012; 111: 1539–1550.
14. Clayton JA, Chalothorn D and Faber JE. Vascular endothelial growth factor-A specifies formation of native collaterals and regulates collateral growth in ischemia. *Circ Res* 2008; 103: 1027–1036.
15. Rissanen TT, Korpisalo P, Markkanen JE, et al. Blood flow remodels growing vasculature during vascular endothelial growth factor gene therapy and determines between capillary arterialization and sprouting angiogenesis. *Circulation* 2005; 112: 3937–3946.
16. Tirziu D, Jaba IM, Yu P, et al. Endothelial nuclear factor-kappaB-dependent regulation of arteriogenesis and branching. *Circulation* 2012; 126: 2589–2600.
17. Ozawa CR, Banfi A, Glazer NL, et al. Microenvironmental VEGF concentration, not total dose, determines a threshold between normal and aberrant angiogenesis. *J Clin Invest* 2004; 113: 516–527.

18. Degenfeld von G, Banfi A, Springer ML, et al. Microenvironmental VEGF distribution is critical for stable and functional vessel growth in ischemia. *FASEB J* 2006; 20: 2657–2659.
19. Greenberg JI, Shields DJ, Barillas SG, et al. A role for VEGF as a negative regulator of pericyte function and vessel maturation. *Nature* 2008; 456: 809–813.
20. Gaengel K, Genove G, Armulik A, et al. Endothelial-mural cell signaling in vascular development and angiogenesis. *Arterioscler Thromb Vasc Biol* 2009; 29: 630–638.
21. Jain RK. Molecular regulation of vessel maturation. *Nat Med* 2003; 9: 685–693.
22. Gianni-Barrera R, Butschkau A, Uccelli A, et al. PDGF-BB regulates splitting angiogenesis in skeletal muscle by limiting VEGF-induced endothelial proliferation. *Angiogenesis* 2018; 21: 883–900.
23. Banfi A, Degenfeld von G, Gianni-Barrera R, et al. Therapeutic angiogenesis due to balanced single-vector delivery of VEGF and PDGF-BB. *FASEB J* 2012; 26: 2486–2497.
24. Gianni-Barrera R, Bartolomeo M, Vollmar B, et al. Split for the cure: VEGF, PDGF-BB and intussusception in therapeutic angiogenesis. *Biochem Soc Trans* 2014; 42: 1637–1642.
25. Gianni-Barrera R, Burger M, Wolff T, et al. Long-term safety and stability of angiogenesis induced by balanced single-vector co-expression of PDGF-BB and VEGF164 in skeletal muscle. *Sci Rep* 2016; 6: 21546.
26. Springer ML, Ozawa CR, Banfi A, et al. Localized arteriole formation directly adjacent to the site of VEGF-induced angiogenesis in muscle. *Mol Ther* 2003; 7: 441–449.
27. Rando TA and Blau HM. Primary mouse myoblast purification, characterization, and transplantation for cell-mediated gene therapy. *J Cell Biol* 1994; 125: 1275–1287.
28. Hecht N, Peña-Tapia P, Vinci M, et al. Myoblast-mediated gene therapy via encephalomyosynangiosis – a novel strategy for local delivery of gene products to the brain surface. *J Neurosci Methods* 2011; 201: 61–66.
29. Hecht N, Marushima A, Nieminen M, et al. Myoblast-mediated gene therapy improves functional collateralization in chronic cerebral hypoperfusion. *Stroke* 2015; 46: 203–211.
30. Springer ML and Blau HM. High-efficiency retroviral infection of primary myoblasts. *Somat Cell Mol Genet* 1997; 23: 203–209.
31. Hecht N, He J, Kremenetskaia I, et al. Cerebral hemodynamic reserve and vascular remodeling in C57/BL6 mice are influenced by age. *Stroke* 2012; 43: 3052–3062.
32. Shen S-W, Duan C-L, Chen X-H, et al. Neurogenic effect of VEGF is related to increase of astrocytes transdifferentiation into new mature neurons in rat brains after stroke. *Neuropharmacology* 2016; 108: 451–461.
33. Duan C-L, Liu C-W, Shen S-W, et al. Striatal astrocytes transdifferentiate into functional mature neurons following ischemic brain injury. *Glia* 2015; 63: 1660–1670.
34. Bethel-Brown C, Yao H, Hu G, et al. Platelet-derived growth factor (PDGF)-BB-mediated induction of monocyte chemoattractant protein 1 in human astrocytes: implications for HIV-associated neuroinflammation. *J Neuroinflammation* 2012; 9: 262.
35. Chapouly C, Tadesse Argaw A, Horng S, et al. Astrocytic TYMP and VEGFA drive blood-brain barrier opening in inflammatory central nervous system lesions. *Brain* 2015; 138: 1548–1567.
36. Stiver SI and Ogilvy CS. Acute hyperperfusion syndrome complicating EC-IC bypass. *J Neurol Neurosurg Psychiatry* 2002; 73: 88–89.
37. Brozici M, van der Zwan A and Hillen B. Anatomy and functionality of leptomeningeal anastomoses: a review. *Stroke* 2003; 34: 2750–2762.
38. Zhang H, Prabhakar P, Sealock R, et al. Wide genetic variation in the native pial collateral circulation is a major determinant of variation in severity of stroke. *J Cereb Blood Flow Metab* 2010; 30: 923–934.
39. Kitagawa K, Matsumoto M, Yang G, et al. Cerebral ischemia after bilateral carotid artery occlusion and intraluminal suture occlusion in mice: evaluation of the patency of the posterior communicating artery. *J Cereb Blood Flow Metab* 1998; 18: 570–579.
40. Mukawa M, Nariai T, Inaji M, et al. First autopsy analysis of a neovascularized arterial network induced by indirect bypass surgery for moyamoya disease: case report. *J Neurosurg* 2016; 124: 1211–1214.
41. Bailey AM, O'Neill TJT, Morris CE, et al. Arteriolar remodeling following ischemic injury extends from capillary to large arteriole in the microcirculation. *Microcirculation* 2008; 15: 389–404.
42. Misteli H, Wolff T, Fuglistaler P, et al. High-throughput flow cytometry purification of transduced progenitors expressing defined levels of vascular endothelial growth factor induces controlled angiogenesis in vivo. *Stem Cells* 2010; 28: 611–619.
43. Cabezas R, Vega-Vela NE, Gonzalez-Sanmiguel J, et al. PDGF-BB preserves mitochondrial morphology, attenuates ROS production, and upregulates neuroglobin in an astrocytic model under rotenone insult. *Mol Neurobiol* 2018; 55: 3085–3095.
44. Pekny M, Wilhelmsson U and Pekna M. The dual role of astrocyte activation and reactive gliosis. *Neurosci Lett* 2014; 565: 30–38.
45. Wang Y, Kilic E, Kilic U, et al. VEGF overexpression induces post-ischaemic neuroprotection, but facilitates haemodynamic steal phenomena. *Brain* 2005; 128: 52–63.
46. He Y, Yu S, Hu J, et al. Changes in the anatomic and microscopic structure and the expression of HIF-1alpha and VEGF of the Yak heart with aging and hypoxia. *PLoS One* 2016; 11: e0149947.
47. Sui H, Zhao J, Zhou L, et al. Tanshinone IIA inhibits beta-catenin/VEGF-mediated angiogenesis by targeting TGF-beta1 in normoxic and HIF-1alpha in hypoxic microenvironments in human colorectal cancer. *Cancer Lett* 2017; 403: 86–97.
48. Dirnagl U. Thomas Willis Lecture: is translational stroke research broken, and if so, how can we fix it? *Stroke* 2016; 47: 2148–2153.